



# CHORUS

This is the accepted manuscript made available via CHORUS. The article has been published as:

## Angular interferences of sequentially ionized double-continuum wave packets

Xiao Wang and F. Robicheaux

Phys. Rev. A **98**, 053407 — Published 8 November 2018

DOI: [10.1103/PhysRevA.98.053407](https://doi.org/10.1103/PhysRevA.98.053407)

# Angular interferences of sequentially ionized double continuum wave packets

Xiao Wang<sup>1</sup> and F. Robicheaux<sup>1,2,\*</sup>

<sup>1</sup>*Department of Physics and Astronomy, Purdue University, West Lafayette, Indiana 47907*

<sup>2</sup>*Purdue Quantum Center, Purdue University, West Lafayette, Indiana 47907*

(Dated: October 11, 2018)

With the recent report of energy and angle interferences in below-threshold photoexcitation Auger process due to the post-collision interactions [*Phys. Rev. A* **98**, 013421 (2018)], similar interferences are also found in double continuum wave packets from a two-step time-delayed photoionization of a two-electron atom. Properties of the interferences are studied in detail with respect to laser pulse time widths, laser frequency chirping, and ionization time delay. The effects of these physical quantities on the resulting interferences are discussed.

## I. INTRODUCTION

The correlations between two electrons in an atom remain an interesting and difficult topic for many years. The Coulomb interaction between the two electrons acts as the most important factor of the coupled degree of freedom in a complex atomic or molecular system. In order to understand the basic interaction between the two electrons, many theoretical and experimental studies have been conducted.

One of the most basic ideas is to study laser induced photoionization of a helium atom. Experimentally, laser induced photoionization has been presented in many previous works [1–8]. Theoretically, many calculations have also been successfully performed [9–14]. Some studies focus on the intrinsic correlations between the two electrons, for example, how the two electrons are ionized or excited by one photon. On the other hand, several authors conducted experiments on probing the two-electron dynamics in an atom [15–17], using sequential two-step laser excitations. In their experiments, barium atoms are prepared in the ground state. First, two consecutive laser pulses excite one of the valence electrons to a coherent Rydberg wave packet. After a short time delay, the other valence electron is also excited to a coherent Rydberg wave packet, possibly with different energy, utilizing the isolated core excitation (ICE) technique [18–21]. Due to the rapid interactions between the two electrons, fast autoionizations can occur in less than one Rydberg period. Time delay of the second excitation gives control over the strength of interaction between the two electrons. Time-resolved observations on the fraction of singly or doubly charged ions act as a probe of the strong interactions between the two electrons. Theoretical calculations on this two-step launch model were performed in a previous study [22] and focused on probing the autoionization of the double Rydberg wave packets.

Another possible way to study the two electron correlation is through the post-collision interaction (PCI) in a laser-induced Auger process. Many theoretical and experimental studies have been performed in the past

decades, e.g. Refs. [23, 24] and references therein. In our previous work [25], we focused on the post-collision interaction in below-threshold photoexcitation Auger processes. Interferences in the distribution of photoelectron energy and relative angle between the two ionized electrons were found. The quantum interferences make visible some of the phase properties of the double continuum wave function. The interference originates from two different classical paths that evolve to the same final energy and relative angle. Properties of this interference were studied using classical trajectories and the classical actions. The semiclassical interference maxima reproduced those from quantum calculations.

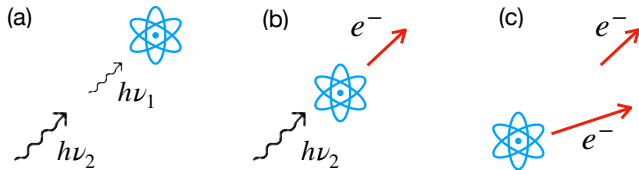


FIG. 1. Cartoon of the two-step ionization model.

Similar to the photoexcitation Auger decay model, simulations also find interferences in the two-step ionization model. In this paper, fully quantum calculations on a two-electron atom are performed, see Fig. 1(a). The first electron is ionized to a spherically symmetric coherent wave packet in the continuum, see Fig. 1(b). After a short time delay, the second electron is ionized to a spherically symmetric coherent wave packet with energy higher than the first wave packet, see Fig. 1(c). After the second electron fully passes the first electron, correlations of the first electron's final energy and the relative angle between the two electrons are evaluated. Effects from properties of the ionization laser pulses on final energy and angle are studied, including time widths and frequency chirpings of the laser pulses. The effects of the variable time delay between the two-step laser ionizations are also investigated. All of the above quantum calculations are interpreted using semiclassical techniques, and detailed analyses are presented on the properties of the interference patterns. Finally, the differences between the two-step ionization model and the photoexcitation

\* robichf@purdue.edu

Auger decay model are discussed in detail.

This paper is structured as follows. In Sec. II, the quantum and classical models used in this paper are briefly introduced. In Sec. III, properties of the interference patterns with different initial conditions are presented. In Sec. IV, discussions of the two models are given. Atomic units are used throughout the paper unless specified otherwise.

## II. METHODS

The two-electron atomic model used in this project has been introduced previously in Refs. [22, 25]. Related experiments have been performed in Ref. [16]. The basic idea of the theoretical model is presented in this section. To reduce the complexity of calculations, both electrons are launched into spherically symmetric radial wave packets, which means their initial angular momentum just after launch is set to zero.

An atom with two active valence electrons, e.g. Ba, is prepared in its ground state. Experimentally, two consecutive short laser pulses are used to excite (or ionize) one of the valence electrons to a coherent radial wave packet. The dynamics of the outgoing ionized electronic wave packet can be described using the following time-dependent inhomogeneous Schrödinger equation [26]:

$$\left[ i \frac{\partial}{\partial t} - (H_1 - E_1) \right] R_1(r_1, t) = S_1(r_1)G_1(t). \quad (1)$$

The  $H_1 = p_1^2/2 + V(r)$  is the Hamiltonian of the first outgoing electron. Although the Coulomb potential  $V(r) = -Z/r$  is used in our calculations, model potentials give very similar results since significant interactions between the two electrons occur away from the nucleus. The potential for the first electron is  $Z = 1$ , before the second electron is ionized.  $R_1$  is the time-dependent radial wave function of the wave packet.  $E_1$  is the central energy of the wave packet.  $S_1$  is source term of the first electron before laser ionization, and it has a small radial extent. The

$$G_1(t) = \exp \left[ -2 \ln(2) t^2 / t_{w,1}^2 - i \dot{\omega}_{c,1} t^2 / 2 \right] \quad (2)$$

is a source term reflecting properties of the laser pulse electric-field used to ionize the first wave packet.  $t_{w,1}$  is the FWHM of the laser pulse, and  $\dot{\omega}_{c,1}$  represents the frequency chirping.

After a variable time delay  $t_d$ , the other valence electron is exposed to a laser pulse with different frequency from the previous excitation, and being excited to another radial wave packet. The dynamics of double wave packets can be calculated using the following time-dependent Schrödinger equation [26]:

$$\begin{aligned} \left[ i \frac{\partial}{\partial t} - (H - E_1 - E_2) \right] \Psi(r_1, r_2, t) \\ = R_1(r_1, t) S_2(r_2) G_2(t). \end{aligned} \quad (3)$$

The  $H = p_1^2/2 + p_2^2/2 + V(r_1) + V(r_2) + 1/r_{12}$  is the full Hamiltonian of the two-electron three-body Coulomb system, and  $E_1, E_2$  are the central energies of the two electronic wave packets, respectively. Here  $Z = 2$  is used in the Coulomb potential term  $V(r)$ .  $\Psi$  is the full two-electron wave function, while  $R_1$  is the radial wave function calculated from Eq. (1).  $S_2$  is the source term with a small radial extent, and

$$G_2(t) = \exp \left[ -2 \ln(2) (t - t_d)^2 / t_{w,2}^2 - i \dot{\omega}_{c,2} (t - t_d)^2 / 2 \right] \quad (4)$$

is a source term reflecting properties of the laser pulse electric-field used to ionize the second wave packet. Similarly,  $t_{w,2}$  is the FWHM of the second laser pulse, and  $\dot{\omega}_{c,2}$  is the frequency chirping. The phase of the second laser pulse relative to the first laser pulse only gives an overall phase shift of the two-electron wave function  $\Psi$ , and has no physical impact to the system.

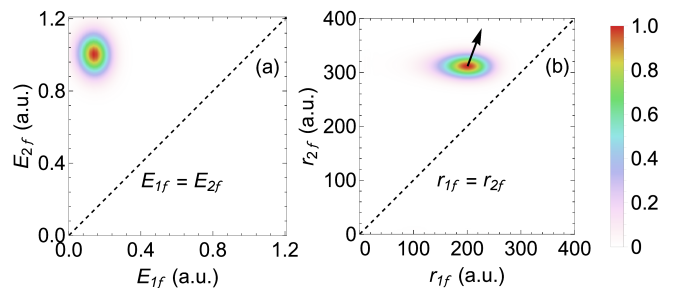


FIG. 2. Final energy and radial distributions from a quantum calculation with initial parameters given in the caption of Fig. 4. The results are non-symmetrized. The final time of the calculation is set to 215 a.u. after the center of the second laser pulse; at this time, the second wave packet has fully passed the first wave packet in position space. The black arrow in figure (b) indicates the moving direction of the wave packet in position space. The separation between the two electrons only gets larger at later times.

It can be seen in Eq. (1) and (3) that the two-electron wave function is non-symmetrized whereas the actual spatial function should be symmetric or anti-symmetric under exchange, depending on the spin coupling. However, all of the calculations below are for cases where the two electrons' energies have relatively large differences which makes them essentially distinguishable. To illustrate this, the final energy and radial distributions from an example quantum calculation are presented in Fig. 2. In neither the energy nor the position representations do the wave functions have overlap with their symmetrized counterpart. Non-symmetrized, symmetrized, or anti-symmetrized wave functions yield nearly identical results in the physical quantities shown in later sections. All results presented in this paper are from non-symmetrized wave functions.

In the expressions for laser pulses in Eq. (2) and (4), the possibility for a substantial chirp has been included for additional control of the two-electron wave functions. There are two important consequences from

the chirp. Firstly, the chirping introduces an energy-dependent phase into the two-electron wave function. For a positive chirping  $\dot{\omega}_c$ , low energy electrons are emitted early; for a negative chirping  $\dot{\omega}_c$ , fast electrons are emitted early. Because of the energy exchange between the two electrons, these relative energy-dependent phases are important. Secondly, when there is frequency chirping, the energy width of the electrons are larger than the minimum from the uncertainty principle. For example, the FWHM of energy distributions are

$$\delta E_j = \left( \frac{4 \ln 2}{t_{w,j}} \right) \sqrt{1 + \left( \frac{\dot{\omega}_{c,j} t_{w,j}^2}{4 \ln 2} \right)^2}, \quad (5)$$

where  $j = 1, 2$  represent the first and the second electron. When  $\dot{\omega}_c t_w^2 = \pm 4\sqrt{3} \ln 2 \approx \pm 4.802$ , the energy width,  $\delta E$ , is doubled from the minimum width without chirping. This provides a tool to study the effect of laser time width or energy width only, without changing the other.

The wave function  $\Psi$  is expanded in a spherical harmonic basis and propagated using the time-dependent close coupling method [26, 27] with an implicit time propagator. The final time of the calculation is chosen such that the second electron's radial wave function fully passes the first electron's. The first electron's energy and the relative angle between the two electrons are evaluated at the final time.

This two-step launch model can also be simulated using the classical trajectory Monte Carlo method [26, 28]. The ionization (launch) times of the electrons are randomly sampled from the quantum source term  $|G_{1,2}(t)|^2$  for each electron. The initial energies are sampled from the Fourier transform of the corresponding launch time distributions. The classical energies  $E_j$  satisfy the following Gaussian distribution:

$$E_j \sim \exp \left( -4 \ln 2 \cdot \left[ E - \tilde{E}_j(t) \right]^2 / \delta E_j^2 \right), \quad (6)$$

where  $j = 1, 2$  represent the first and the second electron. The  $\delta E_j = 4 \ln 2 / t_{w,j}$  is the FWHM of the Gaussian energy distribution *without chirping*. To simulate the frequency chirping, the central energy  $\tilde{E}_j(t) = \tilde{E}_j(0) + \dot{\omega}_{c,j} t$  is time-dependent, where  $\tilde{E}_j(0)$  is the corresponding laser central energy, and  $\dot{\omega}_{c,j}$  is the frequency chirping.

### III. RESULTS

The first calculation is performed with the following initial variables and properties. Each electron's angular momentum just after launch is set to be zero. The initial energies for the two electrons are  $E_1 = 0.15$  a.u.,  $E_2 = 1.0$  a.u. The laser time widths are  $t_{w,1} = 40.0$  a.u.,  $t_{w,2} = 15.0$  a.u., and there is no frequency chirping. The second electron's launch time delay is  $t_d = 120.0$  a.u. At the final time, the relative angle  $\cos \theta$  is defined as the

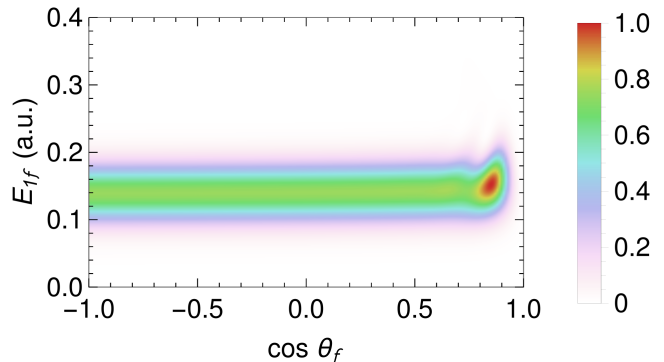


FIG. 3. Distribution of the first electron's final energy versus the final relative angle between the two electrons. The distribution is from quantum calculations. The second electron's final energy is integrated over in the distribution. The initial energies for the electrons are  $E_1 = 0.15$  a.u.,  $E_2 = 1.0$  a.u. The laser widths are  $t_{w,1} = 40.0$  a.u.,  $t_{w,2} = 15.0$  a.u. There is no frequency chirping. The second electron is launched at  $t_d = 120.0$  a.u. after the first electron.

angle between the two electrons' asymptotic momentum at infinity.

Correlation between the first electron's final energy and the relative angle can be found in Fig. 3. Since the launch angular momenta for each of the two electrons are zero, the relative angle  $\cos \theta$  has a flat distribution from  $-1$  to  $1$  if there are no interactions between the two electrons. The interactions between the two electrons are nearly negligible at large relative angle (i.e. small  $\cos \theta$ ), and the distribution presented in Fig. 3 is nearly flat in these regions. However, at a small relative angle (i.e. large  $\cos \theta$ ), when the second electron passes the first electron, the strong repulsion between the two electrons push them away from each other. Thus, nearly no probability can be found at  $\cos \theta_f > 0.95$ , and electrons initially emitted at these relative angles are pushed aside to larger final angles, i.e. smaller  $\cos \theta$ . That makes the relative angle distribution have a local maximum near  $\cos \theta_f \approx 0.87$  and  $E_{1f} \approx 0.15$  a.u. Also, most of those electrons pushed aside gain energy from the strong repulsions, and they can be found in a small tail near  $\cos \theta_f \approx 0.9$  and  $E_{1f} > 0.18$  a.u.

In Fig. 3, another small tail can be found near  $\cos \theta \approx 0.75$  and  $E_{1f} > 0.18$  a.u. which is barely visible. To study the properties of this small tail, quantum calculations are performed with only the first electron's energy width doubled. From the quantum uncertainty principle, this can be achieved by halving the first electron's launch time width  $t_{w,1}$  without introducing any frequency chirping. The distribution of the first electron's energy and the relative angle can be found in Fig. 4. Similar to Fig. 3, the strong repulsion between the two electrons, when they pass close to each other, introduce the vacancy at  $\cos \theta_f > 0.95$ , the local maximum near  $\cos \theta_f \approx 0.87$  and  $E_{1f} \approx 0.15$  a.u., and the first tail near  $\cos \theta_f \approx 0.9$

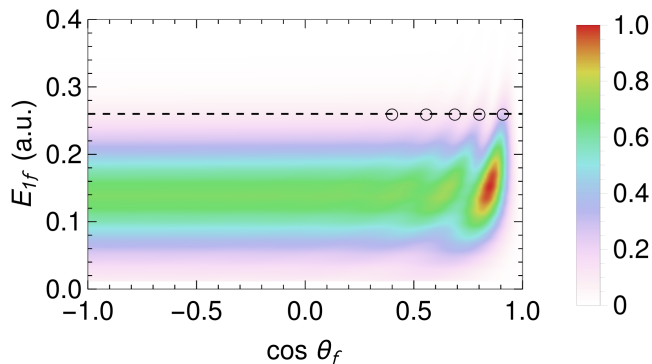


FIG. 4. Distributions of the first electron's final energy versus the final relative angle from quantum calculations. The first electron's launch time width is  $t_{w,1} = 20$  a.u., all other parameters are the same as those given in the caption of Fig. 3. The dashed line is at  $E_{1f} = 0.26$  a.u., while the circles are at the semiclassical interference maxima described later in the text.

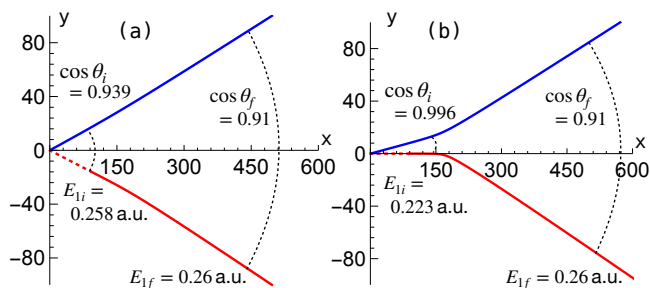


FIG. 5. Illustrations of the two classical trajectories that result in the same final energy and final angle of the first electron. The first electron is indicated by the red line, and the second electron is indicated by the blue line. The dashed red line indicates the motion of the first electron before the second electron is emitted. The launch time delay of the second electron is 120 a.u. The second electron has an initial energy of 1.0 a.u. The figure (a) indicates trajectories with larger initial angle and weaker interaction between the two electrons, while the figure (b) indicates trajectories with smaller initial angle and stronger interaction. The final angle looks larger than  $\cos \theta_f = 0.91$  because the  $x$ -scale is much larger than the  $y$ -scale in the figure.

and  $E_{1f} > 0.18$  a.u. Importantly, a second and a third tail near  $\cos \theta_f \approx 0.8$  and  $0.7$  also are found. The alternations between high and low distributions with respect to  $\cos \theta_f$  are indications of quantum interferences.

To study the properties of these interference patterns, the semiclassical method described in Ref. [25] is used to analyze these classical trajectories. For example, there are two totally different trajectories with final  $\cos \theta_f = 0.91$  and  $E_{1f} = 0.26$  a.u. in Fig. 4. Illustrations of the two trajectories are given in Fig. 5. The first trajectory, as shown in Fig. 5(a), has a larger initial angle between the two electrons' launch directions. The Coulomb interaction between the two electrons in this case is relatively

weak. The final energies and angle is nearly the same as their initial values. The second trajectory, as shown in Fig. 5(b), has a smaller initial launch angle. Since the second electron has a much higher energy than the first electron, intense Coulomb interaction will happen after the late-launched second electron catches up to the early-launched first electron. As can be found from the labels in the figure (b), the first electron gains energy in this process, and gets repelled to a larger final angle. In order for the two trajectories to evolve to the same final energy, the early-emitted electron from the second path must have a much lower energy than the expected final energy. This requires the early-emitted electron be ionized from a laser with a wider energy width, which explains why the interference pattern is stronger in Fig. 4 than in Fig. 3.

When two classical paths have the same final energy and relative angle, quantum interferences may appear [25]. A semiclassical technique is used to calculate the action of the two paths. Note that when the final state is in the momentum representation, an extra phase,  $-\mathbf{p}_{1f} \cdot \mathbf{r}_{1f} - \mathbf{p}_{2f} \cdot \mathbf{r}_{2f}$ , from Fourier transform of the wave function, is added to the total classical action [29–31]. The  $\mathbf{p}_f$  and  $\mathbf{r}_f$  represent the vector momentum and position of the two electrons at a fixed final time. The phase difference between the two paths are used to find the semiclassical interference maxima. For calculations in Fig. 4, the first interference maximum angle is aligned for the semiclassical and quantum calculations, e.g. the  $\cos \theta_f = 0.91$  at  $E_{1f} = 0.26$  a.u. Then, the rest of the interference maxima are found at semiclassical phase difference of  $2\pi$  from the first interference maximum, e.g. the  $\cos \theta_f = 0.80$  at  $E_{1f} = 0.26$  a.u. matched fairly well with the quantum result. The semiclassically calculated interference maxima are marked as circles in Fig. 4.

From calculations in Fig. 3 to calculations in Fig. 4, not only the energy width is doubled, the first electron's launch time width is also halved. In order to study properties of the interference patterns, three quantum calculations are designed with the same energy width but different time widths. This can be achieved by introducing frequency chirping as mentioned in Sec. II and Eq. (5). Correlations of the final energy and the relative angle can be found in Fig. 6. For calculations shown in Fig. 6(a) and (c), the first electron's launch time widths are  $t_{w,1} = 40$  a.u., and frequency chirpings  $\dot{\omega}_{c,1} t_{w,1}^2 \approx \pm 4.802$  are added. Note that the opposite signs in frequency chirping result in a different energy vs launch time distribution for the first electron. As a comparison, the Fig. 6(b) has the same parameters as those in Fig. 4, where its doubled energy width is directly due to the halved time width without frequency chirping. The interference patterns exist in all three calculations, but with slightly different inclines in the distributions of the relative angle. These results verify that the first electron's energy width, but not the launch time width, makes the interference patterns stronger in Fig. 4 than that in Fig. 3.

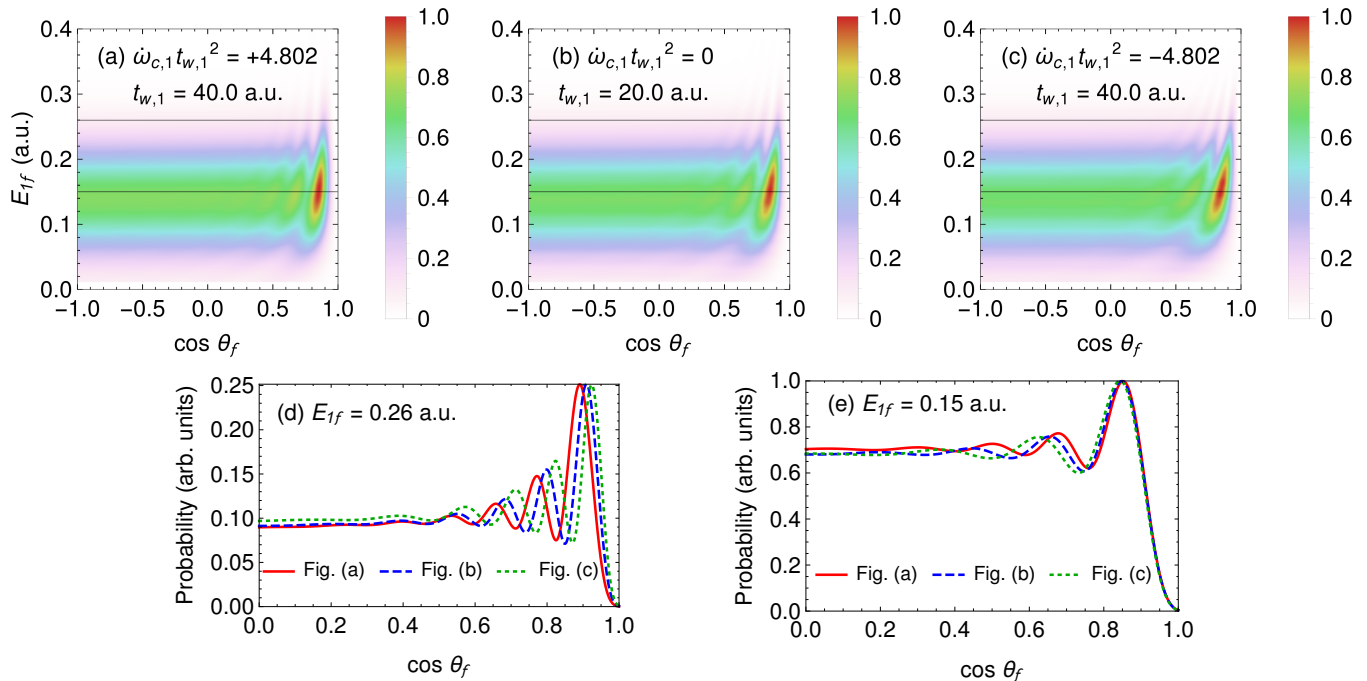


FIG. 6. Comparisons of the first electron's final energy and the relative angle from three quantum calculations are given in (a), (b), and (c). FWHM and frequency chirping properties of the first laser pulse are given in the figure. All other quantities are the same as those given in the caption of Fig. 3. Note that the probability densities are in arbitrary units. Solid lines in the first three figures are plotted at  $E_{1f} = 0.26$  a.u. or  $0.15$  a.u., corresponding to the respective horizontal slices at energies  $E_{1f}$  presented in subfigures (d) and (e).

To study the detailed effects of frequency chirpings in Fig. 6(a-c), the two horizontal slices at  $E_{1f} = 0.26$  and  $0.15$  a.u. are given in subfigures Fig. 6(d) and (e). At high final energy  $E_{1f} = 0.26$  a.u., as chirping  $\dot{\omega}_c$  goes more negative, the interference maxima shift to higher  $\cos \theta_f$ . At low final energy  $E_{1f} = 0.15$  a.u., the maxima shift to lower  $\cos \theta_f$  as  $\dot{\omega}_c$  increases. This can be qualitatively explained that with negative chirping, e.g. in Fig. 6(c), the first electron emitted at an earlier time has higher average energy. Thus, its scattering from the second electron happens at a much further distance from the nucleus, and it is harder for the first electron to be scattered into a larger final angle. As a result, for higher  $E_{1f}$ , the rightmost angle  $\cos \theta_f$  is larger. With negative chirping, the first electron emitted at a later time has lower average energy, and it is more likely to be scattered to larger final angle (i.e. smaller  $\cos \theta_f$ ). The frequency chirpings affect the inclinations of the interference patterns but not the strength of them.

All of the above quantum calculations are performed with the delay time of the second launch being  $t_d = 120$  a.u. Quantum calculations with the delay time being  $t_d = 200$  a.u. are performed. The energy and angle correlation results can be found in Fig. 7. One interesting result for  $t_d = 200$  a.u. is that the interference patterns are more dense than those of  $t_d = 120$  a.u. in the upper right interference region, with respect to the final angle  $\cos \theta_f$ . This can be qualitatively understood that in or-

der to get the same final angle and same final energy, with the first electron being further away from the nucleus, the scattering should be more intense and the first electron gains more energy in this process. To reach the same final energy, the first electron's initial energy has to be much lower, and  $E_{1i}$  decreases much faster versus  $\theta_f$ . Before the second electron is launched, the lower  $E_{1i}$  is, the slower action is accumulated. Then the final total action changes faster as a function of the final angle. Faster oscillations are found in the interference amplitudes with respect to the final angle, with a longer launch delay time.

#### IV. COMPARISONS BETWEEN DOUBLE WAVE PACKETS AND AUGER DECAY MODEL

As discussed in a previous paper [25], quantum interferences also exist in the photoexcitation Auger decay model with post-collision interaction. Different classical trajectories were found that lead to the interferences in the Auger decay model. However, there are several key differences between the Auger decay model and the double wave packets model, and they lead to different interference properties.

The first major difference is the energy widths of the electrons in the two models. In the present double wave packets model, energy widths of the electrons are directly

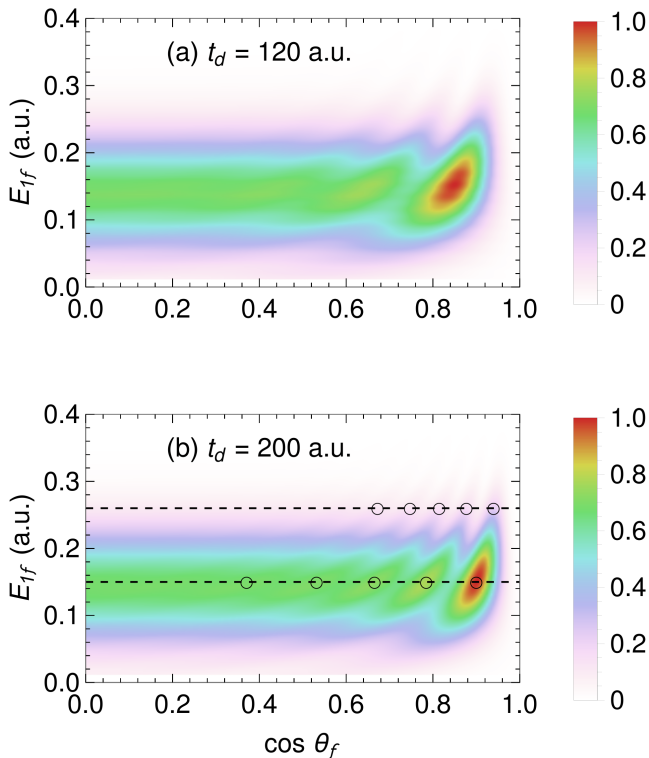


FIG. 7. Distributions of the first electron's final energy versus the final relative angle. The two electrons' launch time widths are  $t_{w,1} = 20.0$  a.u. and  $t_{w,2} = 15.0$  a.u. There is no frequency chirping. The delay times of the second electron's launch  $t_d$  are given in the figure labels. All other parameters are the same as those given in the caption of Fig. 3. Dashed lines in (b) are plotted at  $E_{1f} = 0.26$  a.u. and  $E_{1f} = 0.15$  a.u. while circles are at the semiclassical interference maxima. Note that the  $\cos \theta_f$  range is from 0 to 1.0 in the figure.

controlled by the properties of the laser pulses used to ionize the electrons, and the energy widths can be comparable to the absolute energy of the ionized electrons. In the Auger decay model, the photoelectron's energy width only depends on the lifetime of the inner shell vacancy. This depends on the actual atom considered in the Auger decay. It is often of the order of magnitude around 100 meV [24], which is about  $3.7 \times 10^{-3}$  a.u. That is usually smaller than the absolute energy of the photoelectron, but comparable to the Rydberg spacings. Based on energy conservation, the Auger electron's energy width is the bandwidth of the laser pulse minus the Auger core width. Considering the very high energy of a typical Auger electron, its energy width usually has negligible effect on the final state of the photoelectron.

In the present double wave packets model, the interferences are achieved partly by relatively large energy exchange when the two electrons are launched into small relative angles. However, for the Auger decay model with a positive energy photoelectron, the photoelectron can still be scattered by the later-emitted fast Auger elec-

tron in the two paths as presented in Fig. 5, but the photoelectron will not have the same final energies in the two paths. Interferences with the present two-step launch mechanics thus do not exist in the above-threshold Auger decay model.

The second major difference is the controllable launch time delay between the two electrons. In the Auger decay model, the delay time between the two launches satisfies an exponential distribution. The interference occurs when the Auger core width is equal to or smaller than the adjacent Rydberg spacings of the photoelectron. Locations and oscillations of the interference amplitudes, with respect to the relative angle  $\cos \theta_f$ , mostly depend on the photoelectron energy, but not the Auger core width [25]. The smaller Auger core width only makes the interference patterns brighter. In the present two-step launch model, the delay time is a single tunable value. Locations and oscillations of the interferences mainly depend on this delay time between the two launches. The first electron's larger energy width makes the interference pattern brighter.

As discussed in the final paragraph in Sec. III, in the present two-step launch model, the main difference in total action accumulation is from the the first electron before the second electron emission. This is also true for the below-threshold Auger decay model. In the Auger decay model, the action accumulated by the photoelectron before the Auger decay significantly affects the final interference patterns. For fixed initial and final photoelectron energies, the Auger decay times of the two paths only depend on the final relative angle. Thus the action accumulation differences and oscillations of the interference patterns, with respect to the final relative angle, mainly depend on the initial photoelectron energy, but not the Auger core width.

Last, the tilting direction of the interference patterns with respect to the final angle are studied for the two models. For results presented in the two models, in the correlation of the first electron's final energy and the relative angle, along an interference ridge, both  $\cos \theta_f$  and  $E_{1f}$  go higher or lower, in the same numerical direction. This can be understood that for electrons with higher energy, the scattering usually happens at a far distance from the nucleus. It is then harder for the first electron to be scattered into a larger final angle, or smaller  $\cos \theta_f$ , because the second electron has to be aimed at a very narrow angle relative to the first electron's. As an interesting example presented in Fig. 6(a), due to the laser frequency chirping, the first electron with lower energy is emitted earlier while higher energy is emitted later. With a reasonable delay time, the first electron's wave function can have a very narrow radial width while scattered by the second electron. This causes the final interference pattern be nearly vertical on the  $\cos \theta_f$  scale.

## V. CONCLUSIONS

In this paper, the interferences in the two-step launch double wave packets model were presented. The two-step launch model contains sequentially ionized double wave packets using laser pulses. The two wave packets can have different energies or different energy widths due to the properties of the laser pulses. The delay time between the ionizations of the double wave packets is also tunable in an experiment. Numerical calculations are performed using both quantum and classical methods. The angular momentum of both electrons is set to zero just after launch. At the final time of the calculations, the distribution of the first electron's energy versus the relative angle between the two electrons is studied. At large final relative angle, the distribution is mostly flat, and the final angle is nearly the same as their initial angle. In these regions, the final energies are also nearly the same as their initial energies. However, due to the repulsion between the two electrons, the two electrons initially launched into very close directions are repelled to larger final relative angles. The first electron gains energy in this process. In these two different scenarios, there are two sets of trajectories that start with different initial energies and angles but result in the same final energy and relative angle. Semiclassical action is used

to analyze the two different trajectories and locations of quantum interference maxima. Properties of the quantum interferences are studied in detail with respect to different initial physical parameters, including laser pulse width, laser frequency chirping, and time delay between the two-step ionizations.

Furthermore, the present double wave packet model and the below threshold photoexcitation Auger decay model [25] are compared. Differences in the physical model are discussed, including the fixed tunable delay time between the two-step ionizations in the double wave packet model, versus the exponentially distributed Auger core decay time after photoexcitation. Effects of the initial energy distributions of the two electrons in these two models are also studied. Further studies of these two models can focus on the non-zero initial angular momentum of the two electrons, and novel interference patterns may be discovered.

## ACKNOWLEDGMENTS

This material is based upon work supported by the U.S. Department of Energy, Office of Science, Basic Energy Sciences, under Award No. DE-SC0012193. This research was supported in part through computational resources provided by Information Technology at Purdue University, West Lafayette, Indiana.

- 
- [1] T. A. Carlson, *Phys. Rev.* **156**, 142 (1967).
  - [2] J. A. R. Samson, W. C. Stolte, Z.-X. He, J. N. Cutler, Y. Lu, and R. J. Bartlett, *Phys. Rev. A* **57**, 1906 (1998).
  - [3] T. Carlson, *Photoelectron and Auger Spectroscopy* (Springer US, 2013).
  - [4] V. Schmidt, *Reports on Progress in Physics* **55**, 1483 (1992).
  - [5] F. Wuilleumier and M. O. Krause, *Phys. Rev. A* **10**, 242 (1974).
  - [6] D. M. P. Holland, K. Codling, G. V. Marr, and J. B. West, *Journal of Physics B: Atomic and Molecular Physics* **12**, 2465 (1979).
  - [7] R. Wehlitz, F. Heiser, O. Hemmers, B. Langer, A. Menzel, and U. Becker, *Phys. Rev. Lett.* **67**, 3764 (1991).
  - [8] R. Dörner, H. Bräuning, J. M. Feagin, V. Mergel, O. Jagutzki, L. Spielberger, T. Vogt, H. Khemliche, M. H. Prior, J. Ullrich, C. L. Cocke, and H. Schmidt-Böcking, *Phys. Rev. A* **57**, 1074 (1998).
  - [9] F. W. Byron and C. J. Joachain, *Phys. Rev.* **164**, 1 (1967).
  - [10] A. S. Kheifets and I. Bray, *Phys. Rev. A* **57**, 2590 (1998).
  - [11] E. Fomouo, G. L. Kamta, G. Edah, and B. Piraux, *Phys. Rev. A* **74**, 063409 (2006).
  - [12] P. Selles, L. Malegat, and A. K. Kazansky, *Phys. Rev. A* **65**, 032711 (2002).
  - [13] T. Schneider and J.-M. Rost, *Phys. Rev. A* **67**, 062704 (2003).
  - [14] L. Argenti, R. Pazourek, J. Feist, S. Nagele, M. Liertzner, E. Persson, J. Burgdörfer, and E. Lindroth, *Phys. Rev. A* **87**, 053405 (2013).
  - [15] S. N. Pisharody and R. R. Jones, *Science* **303**, 813 (2004).
  - [16] X. Zhang, R. R. Jones, and F. Robicheaux, *Phys. Rev. Lett.* **110**, 023002 (2013).
  - [17] H. Stapelfeldt, D. G. Papaioannou, L. D. Noordam, and T. F. Gallagher, *Phys. Rev. Lett.* **67**, 3223 (1991).
  - [18] W. E. Cooke, T. F. Gallagher, S. A. Edelstein, and R. M. Hill, *Phys. Rev. Lett.* **40**, 178 (1978).
  - [19] A. ten Wolde, L. D. Noordam, A. Lagendijk, and H. B. van Linden van den Heuvell, *Phys. Rev. Lett.* **61**, 2099 (1988).
  - [20] R. R. Jones, *Phys. Rev. A* **57**, 446 (1998).
  - [21] R. R. Jones, *Phys. Rev. A* **58**, 2608 (1998).
  - [22] X. Wang and F. Robicheaux, *Phys. Rev. A* **96**, 043409 (2017).
  - [23] M. U. Kuchiev and S. A. Shenerman, *Soviet Physics Uspekhi* **32**, 569 (1989).
  - [24] G. B. Armen, H. Aksela, T. Åberg, and S. Aksela, *Journal of Physics B: Atomic, Molecular and Optical Physics* **33**, R49 (2000).
  - [25] X. Wang and F. Robicheaux, *Phys. Rev. A* **98**, 013421 (2018).
  - [26] F. Robicheaux, *Journal of Physics B: Atomic, Molecular and Optical Physics* **45**, 135007 (2012).
  - [27] M. S. Pindzola, F. Robicheaux, S. D. Loch, J. C. Berengut, T. Topcu, J. Colgan, M. Foster, D. C. Griffin, C. P. Ballance, D. R. Schultz, T. Minami, N. R. Badnell, M. C. Witthoef, D. R. Plante, D. M. Mitnik, J. A. Ludlow, and U. Kleiman, *Journal of Physics B: Atomic,*

- Molecular and Optical Physics **40**, R39 (2007).
- [28] Q. Wang and S. D. Loch, Phys. Rev. A **91**, 053416 (2015).
- [29] N. I. Shvetsov-Shilovski, M. Lein, L. B. Madsen, E. Räsänen, C. Lemell, J. Burgdörfer, D. G. Arbó, and K. Tókési, Phys. Rev. A **94**, 013415 (2016).
- [30] K. G. Kay, Annual Review of Physical Chemistry **56**, 255 (2005), pMID: 15929199.
- [31] W. H. Miller, “Classical-limit quantum mechanics and the theory of molecular collisions,” in *Advances in Chemical Physics* (Wiley-Blackwell, 2007) pp. 69–177.